

SS16: X-ray diffraction and X-ray spectroscopy (mini-project)

Lyubomir Shoylev, shil5377

May 6, 2022

Abstract

In this experiment, we study the production of X-ray emission lines and verify Moseley's Law by measuring the energy of emission line series in several metals. Then, we use spectroscopy to report on the composition of different samples: two semiconductors, several unlabelled alloys and international metal coins. We give results for the mass ratios of the unlabelled alloys. We also find that most coins are made up of either Ni-Cu or Cu-Zn alloys and expand on the reasons behind this choice.

1 Introduction

X-rays are an important experimental tool and have been for more than a 100 years, ever since their discovery by Wilhelm Röntgen. They are currently employed by both scientists, from scattering experiments in condensed matter to high-energy astrophysics, and citizens for various medical purposes and security scanners. In this experiment, we first study the theoretical basis of X-ray production, originally developed by Moseley. We measure the energy of the K_{α} and L_{α} emission line series of several samples of known elements with known atomic number, Z , to verify Moseley's Law. Having established the uniqueness of X-ray emission lines for a given Z , we use it to study the composition of several samples provided to us in the laboratory by measuring their emission spectra when exposed to a continuous X-ray source. We begin by independently confirming the composition of two semiconductor samples which was previously obtained using diffraction (see [Appendix A](#)). Then we report on the composition of several unlabelled metal alloys and the relative mass ratios of the samples. Finally, we report on the composition of an array of international coins and expand more on the reasoning for the mainly Ni-Cu-Zn composition.

2 Theory

We begin by introducing some of the background theory behind X-rays and their production.

2.1 X-ray atomic spectra

The emission spectra of atoms is due to energy transitions of shell electrons from a higher- to a lower-energy level. We are interested in X-rays, specifically, which are due to transitions in the inner electron levels of high- Z atoms. These are shielded from the outer electron layers and are mostly unaffected by the chemical structure of the sample i.e. by the surrounding atoms. Therefore, we can take an energy level of an electron to be $E_n = -R(Z)/n^2$ where $R(Z) = R_{\infty}(Z - b)^2$ is the modified Rydberg constant for a given Z , b is an atom-dependent parameter, and R_{∞} is the hydrogen Rydberg constant. Then, the energy of an emitted photon by an electron transition between levels $n_i > n_f$ is given by:

$$\varepsilon = R(Z) \left(\frac{1}{n_f^2} - \frac{1}{n_i^2} \right). \quad (1)$$

We can rewrite this at fixed n_i, n_f (i.e. for a given line) as:

$$\sqrt{\varepsilon} = m \times Z + C, \quad (2)$$

where m , C are constants. This relationship is known as ‘Moseley’s Law’.

The name convention of the low- n energy levels in X-ray notation is given in Table 1. The energy difference between different L, M levels is not large, so if we have a low resolution detector we usually observe e.g. only one K_α line. Consider the example of Iron (Fe), for which we have values of $K_{\alpha 1} = 6404.0062(99)$ eV and $K_{\alpha 2} = 6391.0264(99)$ eV taken from [1]. We can compare that to the FWHM of the detector we use in this experiment, which is about 400 eV in the range of measurement according to [2, Section 6]. The difference in the two K_α components is 13 eV, which is much less, so we do not resolve them.

Initial level	Final level	Siegbahn notation	IUPAC notation
K ($1s_{1/2}$)	L3 ($2p_{3/2}$)	$K_{\alpha 1}$	K-L3
	L2 ($2p_{1/2}$)	$K_{\alpha 2}$	K-L2
	M3 ($3p_{3/2}$)	$K_{\beta 1}$	K-M3
	M2 ($3p_{1/2}$)	$K_{\beta 3}$	K-M2
L3 ($2p_{3/2}$)	M5 ($3d_{5/2}$)	$L_{\alpha 1}$	L3-M5
	M4 ($3d_{3/2}$)	$L_{\alpha 2}$	L3-M4
L2 ($2p_{1/2}$)	M4 ($3d_{3/2}$)	$L_{\beta 1}$	L2-M4
M5 ($3d_{5/2}$)	N7 ($4f_{7/2}$)	$M_{\alpha 1}$	M5-N7

Table 1: Table of the connection between Siegbahn and IUPAC notation. Energy levels in IUPAC are listed with atomic notation as well. Source: [3].

2.2 X-ray production

In practice, we produce X-rays by bombarding a sample of some material with high energy electrons or X-rays which removes one of the inner shell electrons from the sample atom. This produces a vacancy in the shell. The vacancy is filled by an electron of a higher- n orbit (see Figure 1), and the fall of potential energy of the electron is compensated by an emitted X-ray (ignoring higher order effects like the *Auger effect*).

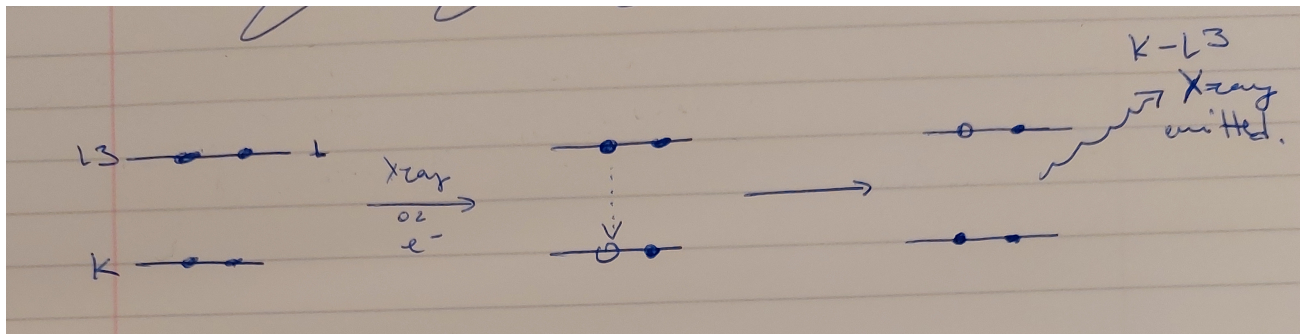


Figure 1: Schematic of the emission process for a K-L3 transition.

Usually, small laboratory X-ray tubes use an electron source. Because of that, we observe a continuum of X-ray radiation imposed on top of the emission lines. This radiation is called *bremsstrahlung* (“braking”) radiation. Its source is the interaction between decelerating electrons and stationary charges in the sample lattice. The maximal energy of a bremsstrahlung continuum is limited by the energy of the decelerating particle. If these are electrons accelerated by a potential difference V , then the maximal energy is given by:

$$\varepsilon_{\max} = eV. \quad (3)$$

Suppose we use one such continuous X-ray source for the production of X-rays from a sample. We will take the K-series as an example. To produce a vacancy, an X-ray of energy $\varepsilon_{\text{in}} = -E_1 = R(Z)$ is needed, which will be provided by a collision with an electron with maximum energy ε_{\max} in the case of the X-ray source. The resultant energy of the emitted X-ray will be given by Equation (1). Take,

for example, the K-L transition: its energy will therefore be (ignoring fine-structure):

$$\varepsilon_{\text{out}} = R(Z) \left(1 - \frac{1}{2^2}\right). \quad (4)$$

A process like this, in which $|\varepsilon_{\text{in}}| \neq |\varepsilon_{\text{out}}|$, is called *fluorescence*.

2.3 Composition analysis

As previously stated, the X-ray emission is relatively independent of the composition of the sample. We can use this fact to perform a composition analysis on a sample by exposing it to the continuous bremsstrahlung of a source; this will allow the different constituents to fluoresce. The signal will give us information not only about *which* elements are present (given that the source is high enough to allow fluorescence), but their relative contribution — the intensity of the signal will depend only on the number density, n . Suppose we measure the intensity of a two-metal alloy with the peaks in the K_{α} line as I_A and I_B . This tells us that:

$$\frac{I_A}{I_B} = \frac{n_A}{n_B}, \quad (5)$$

where n_A and n_B are the number densities of materials A and B. From that, we could easily calculate percentage compositions for number densities or mass densities:

$$\rho = n \times \mu, \quad \mu = \text{molar mass}. \quad (6)$$

3 Experiment

Our experiment consists of the setup presented in Figure 2. First, we have an X-ray source with a Mo (molybdenum) anode, which produces some characteristic K_{α} X-rays that can be used for diffraction experiments (more details in [4]; key results are presented in Appendix A) and a continuum spectrum called bremsstrahlung (see Section 2.2 for more details). These X-rays are focused through a circular aperture towards a target sample. The incident X-rays excite inner shell electrons, and the targets emit mostly in the characteristic X-rays of K, L, and M series. We detect these via an energy spectrometer that is sensitive in the region of our experiment (see [2]). The setup parameters are: tube voltage $V = 35$ kV, emission current 1 A, exposure time $t = 100$ s. This, according to Equations (3) and (4), allows us to produce, for example, K_{α} X-rays with energy up to 26.25 keV from samples with atomic numbers up to at least 50, ignoring the contribution from b .

To operate the apparatus and extract data, we use the software *CASSY Lab 2* (see [5]). The program has a built in database for the X-ray emission lines of most elements. It also allows for calculating a peak centre and fitting Gaussian profiles with specified energy to find the intensity of emission lines. While the natural broadening of X-rays is asymmetrical, according to [6] the natural linewidths of e.g. Fe K_{α} level is FWHM ≈ 2 eV. On the other side, the experimental accuracy is FWHM ≈ 400 eV for our values. Therefore, we can go ahead and use Gaussian fitting as a first approximation to the observed emission lines.

3.1 Energy scale calibration

Before determining the energies, we first need to calibrate the energy scale. We will use two known samples - Fe and Ag. We choose these two samples since their K_{α} lines lie at the two ends of the range of energies for which our samples have emission lines. The particular lines which we use to calibrate are the Fe K_{α} with $E_{\text{Fe}} = 6.40$ keV and the Ag K_{α} with $E_{\text{Ag}} = 22.17$ keV. Also note the observational lower and upper limits, respectively 2 keV to 4 keV and ≈ 35 keV (since the tube voltage is 35 keV). The calibration spectra are presented in Figure 3.

3.2 Experimental errors

We have to also try to estimate the experimental error of the measured intensity I , which is given in counts i.e. the number of detected X-rays at the given energy.

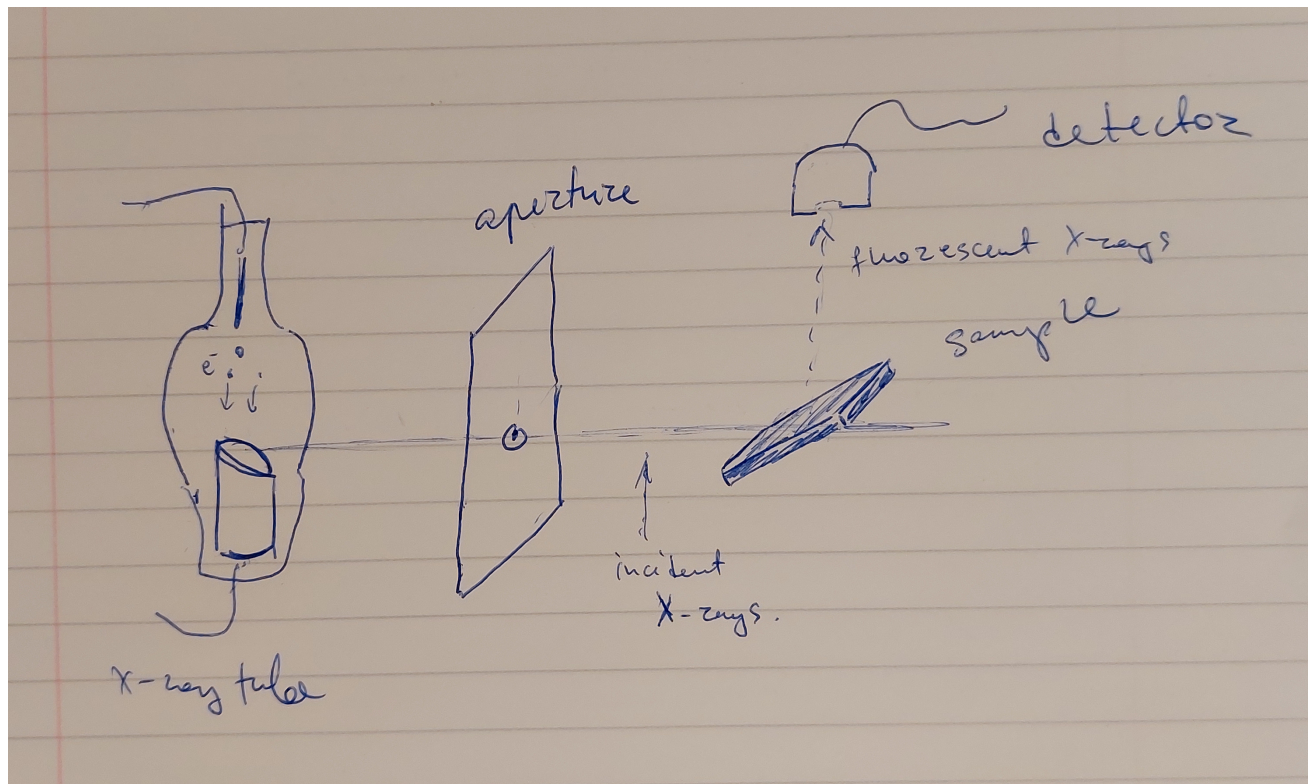


Figure 2: Diagram of the experimental setup. More information can be found in the text of Section 3.

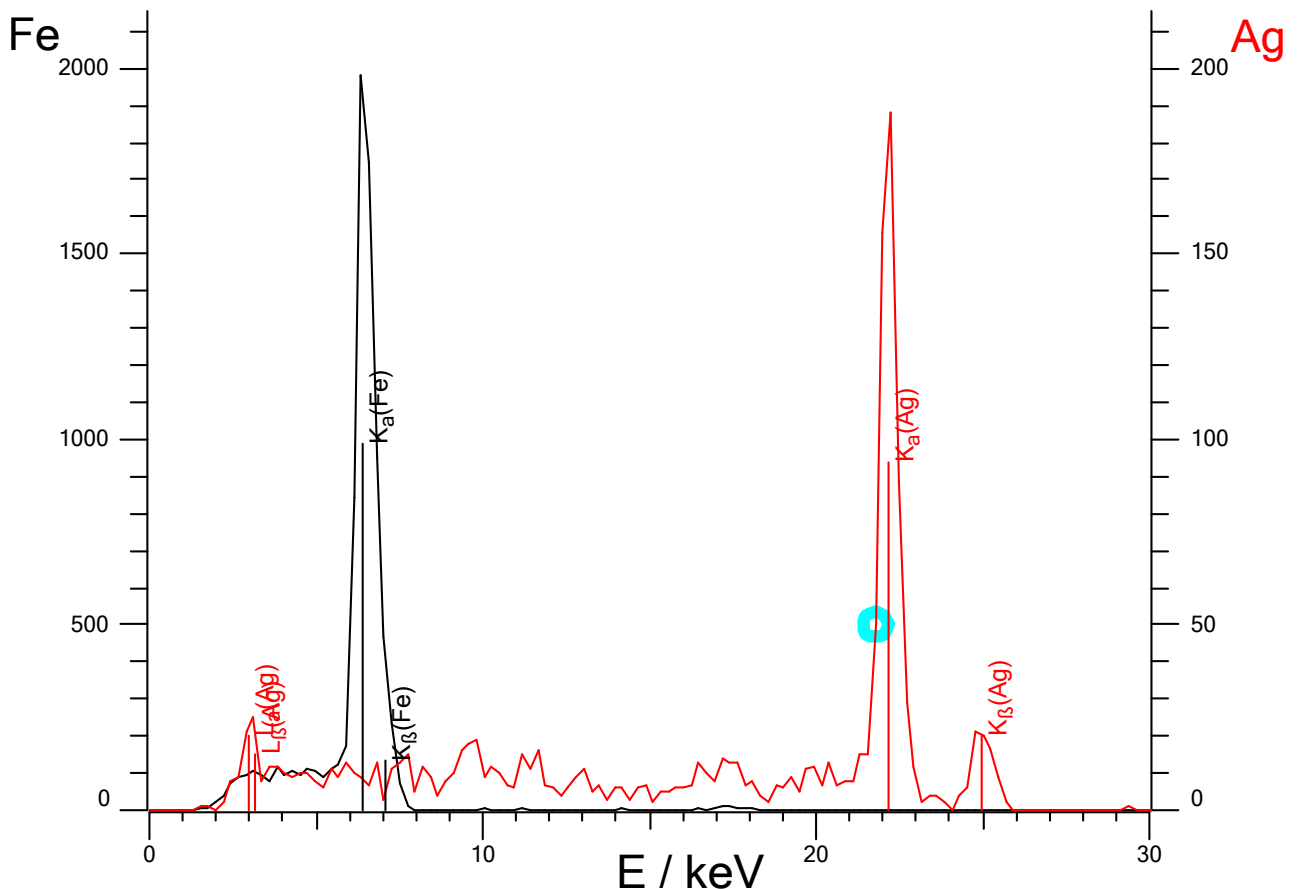


Figure 3: Fe (in black) and Ag (in red) measured spectra used for calibration. On the x-axis, we have the energy of the detected signal ε in keV. On the left and right y-axes, we have the signal counts for the Fe and Ag spectra respectively. The vertical line labels are part of the built-in database of the software *Cassy Lab 2*.

First, we note the background radiation detected for the range 3 keV up to the K_α energy. After examining all spectra, we notice it is $\approx 5\%$ of the K_α line intensity in all spectra. We can use this as a very rough estimate of the uncertainty in the measurements for the K_α intensities, which we apply in Section 4.2.

Second, we also have to note the detector efficiency, which varies greatly across the useful part of the spectrum. The exact relationship is given in [2, Section 3]. This will be of interest especially when measuring quantities for which the K_α lines lie in the range of 5 keV to 15 keV, where the steep decrease in efficiency can impact measurements significantly. We cannot correct for this in a meaningful way, however, since we do not have the functional form of the efficiency.

Lastly, we also note the linearity of the detector given in [2, Section 5] in the range 3 keV to 35 keV is $< 1\%$, so this is a smaller effect than the two other effects.

The first part of the experiment will test the validity of Moseley's Law making use of several samples of known substances.

The second part and third part of the experiment will utilise our knowledge about X-rays to learn more about the composition of other samples, and about some metal coins from around the world.

4 Result and Analysis

4.1 Moseley's Law

We measure the line energy values from the labelled samples. We can separate these in two groups:

- those whose K_α lines lie in the observable range (excluding our two calibration points);
- those whose L_α lines lie in the observable range.

Recalling Equations (1) and (2), we expect to fit the data for the two groups with a straight line for each group. The slope m depends purely on the line we are observing, i.e. on the n_i, n_f for the given line. We can predict the ratio of the constants for the two series. Following Equations (1) and (2), we get:

$$m_K = \sqrt{R_\infty} \left(1 - \frac{1}{2^2}\right)^{1/2} \propto \sqrt{\frac{3}{4}}, \quad m_L = \sqrt{R_\infty} \left(\frac{1}{2^2} - \frac{1}{3^2}\right)^{1/2} \propto \sqrt{\frac{5}{36}} \quad \Rightarrow \quad \frac{m_K}{m_L} = \sqrt{\frac{27}{5}}. \quad (7)$$

Figure 4 shows the fits for the two series. We can see that the data is fitted well by the model provided by Equation (2), given the experimental precision. We can therefore proceed to use X-ray K and L series lines as a signature of a given element in spectral analysis.

The ratio can also be calculated from the fitted values for the slopes, giving:

$$\text{predicted: } \frac{m_K}{m_L} = \sqrt{\frac{27}{5}} = 2.324, \quad \text{observed: } \frac{m_K}{m_L} = \frac{0.1026}{0.0411} = 2.496. \quad (8)$$

While the slope ratio is about 7% off of the value predicted by theory, we have good linear fits for the K_α and L_α series. The difference can be attributed to a modification to the multiplicative constant.

4.2 Provided alloys and semiconductors

We continue with the spectroscopic analysis of two semiconductor samples and several unlabelled samples.

4.2.1 Semiconductors

We have previously determined the composition of the semiconductor samples by measuring the lattice constant (see Appendix A). Here, we will provide an independent confirmation of these results, as well as measure the relative composition.

The spectra of semiconductor samples X2 and Y2 are presented in Figure 5. First, both spectra show a strong K_α line of In, a group III element. There is also a weak signal at the K_α for Mo, which is just the signature of the anode in the X-ray source, so we can ignore it. We also have to note other two features:

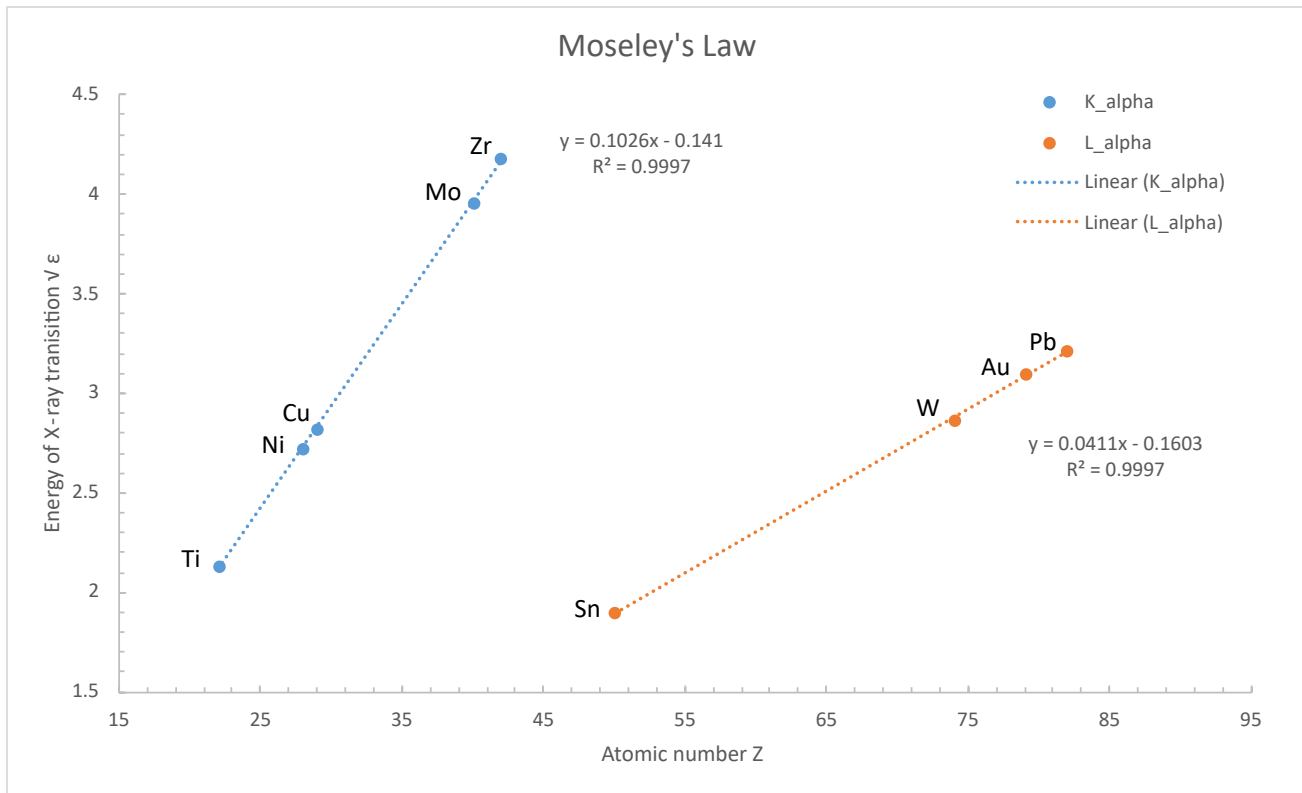


Figure 4: The figure shows a plot of measured $\sqrt{\epsilon}$ vs Z for the samples, listed in order of increasing Z : Ti, Ni, Cu, Mo, Zr for the K_α series and Sn, W, Au, Pb for the L_α series. The elements have also been labelled on the plot. We have applied a linear fit to the two groups of data; the fit formula is also displayed next to the fitted line.

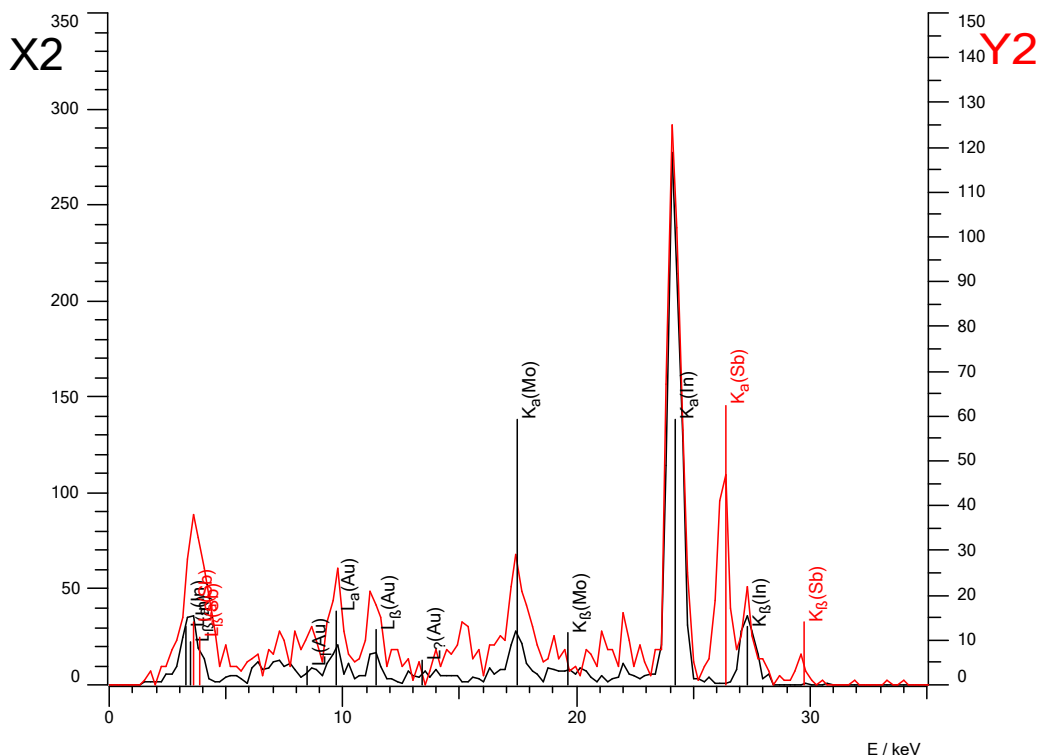


Figure 5: Measured fluorescence spectra of the semiconductors labelled as X2 and Y2. The vertical line labels are part of the built-in database of the software *Cassy Lab 2*. More information about the sources of these lines in the main text of Section 4.2.1.

- the L_α peak at the cyan circle, where the L_α lines for several elements lie;
- the small peaks around 10 keV, which are caused by fluorescence from the detector materials [2, Section 9]. These particular lines are fluorescence lines of gold (Au), as marked in Figure 5.

Semiconductor Y2 also shows traces of Sb, a group III and V elements respectively. This is a very common structure for semiconductors, so this is reassuring. In addition, this confirms our result from [Appendix A](#). We can measure intensities of the K_α lines for both, and calculate the ratios according to Equation (5):

$$\frac{n_{In}}{n_{Sb}} = \frac{I_{In}}{I_{Sb}} = \frac{122.5(61)}{42.8(21)} \approx 2.86(20) \Rightarrow p_{In} = \frac{n_{In}}{n_{In} + n_{Sb}} = 0.74(7) \quad p_{Sb} = 0.26(3). \quad (9)$$

For sample X2, we see a trace of In only. Checking with our result from the diffraction analysis from [Appendix A](#), we see that the dopant is P (phosphorus). The characteristic X-rays of P in K-series (the most energetic ones of a given element) have energies around 2 keV, which is around our detection limit of about 2 keV to 4 keV. This highlights one of the shortcomings of our method: it is limited in detecting only those elements, which have X-ray emission lines in the range of the bremsstrahlung and the range of operation of the detector.

4.2.2 Unlabelled alloys

We continue with measuring the fluorescence spectra of several unlabelled samples. We can determine their relative composition by following the procedure described in Section 2.3, in particular Equation (5). Results are presented in Table 2.

We can first check for consistency of the fits by looking at the ratios of intensities for K_α and K_β , which should be approximately the same for all samples as it depends on the structure of the individual atom. Samples b2-c,d,f have close values for both the Fe and Zn lines. Since these two elements do not overlap in the spectrum (as seen in Figure B4), these ratios should be close to the true ratio. We would expect to observe similar ratios in the other samples for Fe and Zn.

For sample b1-1, the Fe ratio is a little above 4, so we can say that the fit was pretty good. For samples b1-2,3, the Zn ratio is nearly twice the one measured above. The fit here is pretty poor since Cu and Zn are respectively $Z = 29$ and $Z = 30$. Their spectra overlap by a lot (as seen in Figure B3) — the K_α of Zn with $\varepsilon = 8.63$ keV is between K_α with $\varepsilon = 8.03$ keV and K_β with $\varepsilon = 8.91$ keV of Cu (similarly, we can see the overlap for Fe and Cr in the spectrum of sample b1-1 in Figure B2). This, combined with the low resolution of our detector, makes it pretty difficult to fit here. Nevertheless, the K_α lines are much stronger, so we can still try to extract the composition of the alloys.

Alloy composition is usually presented by mass in practical applications. These results are in the last column of Table 2.

4.3 International coins

At last, we analyse various coins from around the world, the content of which we can again interpret using our fluorescence method, similar to the analysis in Section 4.2.2.

The results are summarised in Table 3. When looking at plots of the spectra, we see that almost all coins are made predominantly out of Ni, Cu, and Zn with $Z = 28$ to 30 respectively. The spectra are overlapping, so similarly to the b1-2,3 samples in Section 4.2.2, we cannot really fit the samples well for all α, β pairs. Nevertheless, we can still determine if one of the three elements is present. Additionally, we note down any additional features of the spectra that may be of interest. Two exceptions to the general rule are notable - the 1 Yen and 25c Canadian coins. We can compare our results with the information from the institutions that issue these coins, given in Table C1.

The official information lists the 1 Yen coin to be made of 100% aluminium according to [7]. The K_α line for aluminium is at 1.49 keV, out of the range of our setup. This is the reason we do not see any signal in our spectrum.

The official information informs us that the 25c Canadian coin is a 94% steel core with 6% Ni-Cu plating according to [8]. When we look at the spectrum, however, the strength of the Fe line is much less than the Ni and Cu. This is due to the fact that the X-rays do not penetrate deeply into the coin.

Sample	Element	Line	I	$I(K_\alpha)/I(K_\beta)$	n_A/n_B	n/n_{tot}	ρ/ρ_{tot}
b1-1	Cr	K_α	381.9(191)	5.55(39)	0.42(3)	0.30(3)	0.28(3)
b1-1	Cr	K_β	68.8(34)				
b1-1	Fe	K_α	903.1(452)	4.14(29)		0.70(7)	0.72(7)
b1-1	Fe	K_β	218.2(109)				
b1-2	Cu	K_α	2110.2(1055)	6.14(43)	1.78(13)	0.64(6)	0.69(7)
b1-2	Cu	K_β	343.9(172)				
b1-2	Zn	K_α	1182.9(591)	17.09(121)		0.36(4)	0.31(3)
b1-2	Zn	K_β	69.2(35)				
b1-3	Cu	K_α	3947.9(1974)	14.33(101)	1.27(9)	0.56(6)	0.61(6)
b1-3	Cu	K_β	275.5(138)				
b1-3	Zn	K_α	3119.6(1560)	16.51(117)		0.44(4)	0.39(4)
b1-3	Zn	K_β	188.9(94)				
b2-c	Fe	K_α	1351.9(676)	3.74(26)	2.06(15)	0.67(7)	0.69(7)
b2-c	Fe	K_β	361.8(181)				
b2-c	Zn	K_α	655.6(328)	8.57(61)		0.33(3)	0.31(3)
b2-c	Zn	K_β	76.5(38)				
b2-d	Fe	K_α	1443.6(722)	3.92(28)	3.42(24)	0.77(8)	0.79(8)
b2-d	Fe	K_β	368.1(184)				
b2-d	Zn	K_α	421.9(211)	9.74(69)		0.23(2)	0.21(2)
b2-d	Zn	K_β	43.3(22)				
b2-f	Fe	K_α	1443.3(722)	3.89(27)	2.56(18)	0.72(7)	0.74(7)
b2-f	Fe	K_β	371.5(186)				
b2-f	Zn	K_α	563.9(282)	9.37(66)		0.28(3)	0.26(3)
b2-f	Zn	K_β	60.2(30)				

Table 2: Table of the fitted intensities in alloy samples. Some of the measurements made had signal comparable with the background due to a human error during data acquisition; included here for completeness. The error on n/n_{tot} and ρ/ρ_{tot} is on the order of 10%.

No	Country	Denomination	Ni	Cu	Zn	Other
3	United Kingdom	50p old	yes	yes	no	no
4	United Kingdom	50p new	yes	yes	no	no
5	United Kingdom	20p new	yes	yes	no	no
6	United Kingdom	10p old	yes	yes	no	no
7	United Kingdom	10p new	yes	no	no	no
8	United Kingdom	2p new	no	yes	no	no
9	Singapore	1 dollar old	yes	yes	no	no
10	Singapore	50c old	yes	yes	no	no
11	Singapore	20c new	yes	no	no	no
12	Bulgaria	50 stotinki	yes	yes	yes	no
13	Bulgaria	5 stotinki	no	yes	no	no
14	European Union	50c	no	yes	yes	no
15	European Union	2c old	no	yes	no	no
16	European Union	2c new	no	yes	no	no
17	Romania	10 bani	yes	no	no	no
18	Norway	1 krone	yes	yes	no	no
19	Switzerland	20 centim	yes	yes	no	no
20	Sweden	1 krona	yes	yes	no	no
21	Japan	1 yen	no	no	no	no
22	Hong Kong	10c	no	yes	yes	no
23	Uganda	200 schillings	yes	yes	no	no
24	USA	25c	yes	yes	no	no
25	USA	1c	no	yes	yes	no
26	Canada	25c	yes	yes	no	Fe?
27	Brazil	5 centavos	no	yes	no	no

Table 3: Table of measured metal composition for a selection of international coins.

If a thick enough coating is applied, we could even fully shield the steel core. In fact, several coins on our list follow this pattern, e.g. the new 2p and 10p coins.

4.3.1 Why Ni, Cu, Zn?

One obvious question that comes up from these results is why are alloys of Ni, Cu, and Zn the predominant choice for coin production? There are several properties of these alloys that make them preferable for this task.

Historically, coins were most often made from gold, silver, and copper, with their value determined and guaranteed by the value of the metal in the coin. With the inflation of prices, however, the metal in the coins gradually became more expensive than their monetary value. There was a need for new materials to be implemented while keeping many of the familiar and useful properties of old coins.

Firstly, there are visual considerations of the coins. Ni-Cu and Cu-Zn alloys can have varying colours depending on the ratio of elements used. Ni-Cu are usually silver in appearance, while Cu-Zn alloys are usually golden in appearance, with small amounts of other additives sometimes present, like in the case of the *nordic gold* alloy used for the make of the 50 euro cent coin (see Table C1).

Secondly, the cost considerations required some inexpensive materials to be used so that mass production is practical and coins are not produced at a loss. Due to inflation, this has also led to the change of coin composition throughout the years. One example is the UK 10p coin. While the old coin was made from pure Ni₂₅Cu₇₅, the new coin is made from 94% steel clad in 6% Ni. The method of implementing a cheaper core while using Ni, Cu, Zn for an outer layer also keeps the appearance the same or similar, which is one of the reasons for the approach.

Thirdly, the minting of the coins includes making the alloys and producing the coins with intricate detailing on their surfaces. The alloying of the specific ratios required by the specifications can be a difficult task outside of the specialised large scale industrial complexes. The three metals also allow for the detailing on different designs — their alloys have been used to produce detailing by artisans for millennia. Both of these specifics make the production of good counterfeit coins more difficult, which brings more security to the currency.

Moreover, these alloys are very practical for everyday use. Coins, in their daily use, are exposed to the elements and physical wear. These alloys are very resistant to rusting (although Ni-Cu are often subject to formation of *patina*) and have high durability against physical stresses like bending, stretching etc. This is another reason for the cladding method — this gives them resistance against the elements and the physical toughness also helps preserve the detailing on the surface. The surface of coins made from these three materials are also resistant against microbial growth (see [9]), which is important for public health and safety.

We also have to note that, despite the many advantages these material offer, they do come with some potential drawbacks, again, regarding the public health. For example, the Ni coins can elevate allergies among the general population — studies on this topic include [10], which focuses on the ‘new’ UK nickel coins series from 2008, and [11], which focuses on nickel allergies related to coins in circulation worldwide.

5 Conclusions

In this experiment, we first study the theoretical basis of X-ray production originally developed by Moseley. We measure the energy of the K _{α} and L _{α} emission line series of several samples of known elements with known atomic number $Z = 22$ to 40 and 50 to 82, respectively. We find that there exists a linear relationship between the square root of the energy and number Z as predicted by Moseley’s law. Having established the uniqueness of X-ray emission lines for a given Z , we use them to study the composition of several samples by measuring their emission spectra when exposed to the continuous X-ray source. For the two semiconductors, we observe traces of In in sample X2 and traces of In and Sb in sample Y2, which confirms the independently derived results form diffraction (see Appendix A). We also note the observational limitations of our setup, since the dopant of X2 was not observed — P has a K _{α} of energy below the observational limit.

Then, we study various metal alloys of unknown composition and the relative mass ratios of these samples. We measure these by performing Gaussian fits using the built-in capabilities of the acquisition software. We also perform some analysis to confirm our observations are self-consistent by comparing the ratios of intensities of K_{α} to K_{β} for the same elements in different samples.

Finally, we report on the composition of an array of international coins. We discover that most have signs of Ni, Cu, and Zn in their spectra, predominantly. While it is difficult to exactly extract intensities of the lines since they overlap, we report on the presence of either element in the coins in addition to any other element seen in the spectra. We discuss some seemingly anomalous results, like the 1 Yen and 25c Canadian coins, which turn out to be 100% aluminium and Ni-Cu clad steel. We conclude with a discussion about the frequency of use of these three metals, as well as the need to produce steel-core coins.

There are several directions in which the results of the report can be improved on, including, but not limited to:

- Take into account the spectrum of the bremsstrahlung: in this report we considered it to be approximately flat, while it decreases with energy. This has an impact on the observed intensities.
- Improve/optimise the exposure times depending on the sample: as already noted in Section 3.2, the detector efficiency varies greatly across the spectrum, which contributes to both lower detected signal, and differences in line intensities. An example of that would be to increase the exposure time of the semiconductor samples to get signal of about 2000 counts. This will help with providing more accurate values and removing stray effects, like the detector fluorescence on which we reported in Section 4.2.1.
- Correct for the detection efficiency of the detector to get the true fluorescence intensities.

References

- [1] Lawrence Hudson. *X-ray Transition Energies, NIST Standard Reference Database 128*. en. 2003. DOI: [10.18434/T4859Z](https://doi.org/10.18434/T4859Z).
- [2] LD Didactic GmbH. *Instruction sheet 559 938*. LD Didactic GmbH. 2005. URL: https://www.ld-didactic.de/documents/en-US/GA/GA/5/559/559938e.pdf?_ga=2.102154309.530245957.1650838453-1808266661.1650206614.
- [3] R. Jenkins et al. “Nomenclature, symbols, units and their usage in spectrochemical analysis - VIII. Nomenclature system for X-ray spectroscopy (Recommendations 1991)”. In: *Pure and Applied Chemistry* 63.5 (Jan. 1991), pp. 735–746. DOI: [10.1351/pac199163050735](https://doi.org/10.1351/pac199163050735).
- [4] Oxford Physics. *SS16: X-ray diffraction*. Oxford Physics. Oct. 2010.
- [5] LD Didactic GmbH. *Cassy Lab 2*. Version 2.24.10378. 2010–2021. URL: <https://www.ld-didactic.de/en/products-solutions/data-logging-and-measuring-technology/cassy-software.html>.
- [6] M. O. Krause and J. H. Oliver. “Natural widths of atomic K and L levels, K_{α} X-ray lines and several KLL Auger lines”. In: *Journal of Physical and Chemical Reference Data* 8.2 (Apr. 1979), pp. 329–338. DOI: [10.1063/1.555595](https://doi.org/10.1063/1.555595).
- [7] Japan Mint. *Coins Presently Minted*. URL: https://www.mint.go.jp/eng/operations-eng/production-eng/production-aproach-eng/eng_operations_coin_index.html.
- [8] Royal Canadian Mint. *A familiar face – the 25-cent coin*. URL: <https://www.mint.ca/store/mint/learn/25-cents-5300010>.
- [9] Frank Vriesekoop et al. “Dirty Money: A Matter of Bacterial Survival, Adherence, and Toxicity”. In: *Microorganisms* 4.4 (Nov. 2016), p. 42. DOI: [10.3390/microorganisms4040042](https://doi.org/10.3390/microorganisms4040042).
- [10] Anneli Julander et al. “New UK nickel-plated steel coins constitute an increased allergy and eczema risk”. In: *Contact Dermatitis* 68.6 (May 2013), pp. 323–330. DOI: [10.1111/cod.12092](https://doi.org/10.1111/cod.12092).

- [11] Carsten R. Hamann et al. “The cost of nickel allergy: a global investigation of coin composition and nickel and cobalt release”. In: *Contact Dermatitis* 68.1 (Dec. 2012), pp. 15–22. DOI: [10.1111/cod.12008](https://doi.org/10.1111/cod.12008).
- [12] The Royal Mint. *Coin Designs and Specifications (online article)*. URL: <https://www.royalmint.com/discover/uk-coins/coin-design-and-specifications/>.
- [13] Board of Commissioners of Currency. *Currency Notes and Coins (Consolidation) Notification*. Mar. 1992. URL: <https://sso.agc.gov.sg/SL/69-N1?DocDate=19920325&ProvIds=Sc-&Timeline=On#Sc->.
- [14] Board of Commissioners of Currency. *Currency (Denominations and Characteristics of Coins) (No. 3) Notification 2015*. Dec. 2015. URL: <https://sso.agc.gov.sg/SL/CA1967-S780-2015?DocDate=20151223&ProvIds=Sc-#Sc->.
- [15] “Council Regulation (EU) No 729/2014 of 24 June 2014 on denominations and technical specifications of euro coins intended for circulation (Recast)”. In: *Official Journal of the European Union* L 194 (June 2014), pp. 1–7. ISSN: ISSN 1977-0677. URL: <https://eur-lex.europa.eu/legal-content/EN/TXT/?uri=OJ:L:2014:194:TOC>.
- [16] Norges Bank. *1-krone coin - Design and technical specifications*. Sept. 1997. URL: <https://www.norges-bank.no/en/topics/notes-and-coins/legal-tender-notes-coins/1-krone-coin/1-design/>.
- [17] Wikipedia. *Coins of the Swiss franc*. URL: https://en.wikipedia.org/wiki/Coins_of_the_Swiss_franc.
- [18] Sveriges Riksbank. *Invalid 1-krona coin*. 2017. URL: <https://www.riksbank.se/en-gb/payments--cash/notes--coins/coins/invalid-coins/invalid-1-krona-coin/>.
- [19] Hong Kong Monetary Authority. *Coins in Circulation*. URL: <https://www.hkma.gov.hk/eng/key-functions/money/hong-kong-currency/coins/>.
- [20] United States Mint. *Coin Specifications*. 2019. URL: <https://www.usmint.gov/learn/coin-and-medal-programs/coin-specifications>.

Appendix A X-ray diffraction

The first part of the practical featured several experiments in X-ray diffraction. X-rays undergo diffraction in crystals according to Bragg's Law:

$$n\lambda = 2d \sin \theta \quad (10)$$

with λ the wavelength of the incident X-ray, d the interplanar crystal spacing, θ the angle of the ray to the crystal plane, and n some integer value. This means the angle between the incident and diffracted beam is 2θ .

In our setup (see left of Figure A1) we have a fixed molybdenum X-ray source which emits a characteristic K_{α} X-ray. We can use this fixed X-ray wavelength in our diffraction experiment to determine the value of the lattice constant a for some sample. We scan the diffracted intensity as a function of θ by simultaneously rotating the sample by θ and the detector by 2θ . An example can be seen on the right of Figure A1. We can therefore fit $n\lambda$ vs $\sin \theta$ to find the value of d .

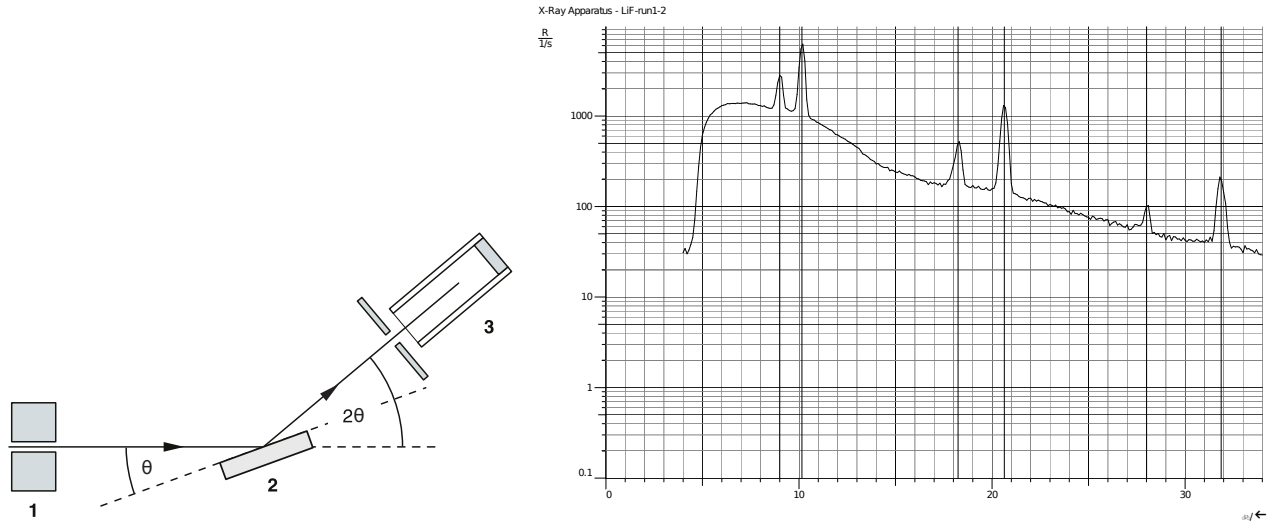


Figure A1: **Left:** Diffraction setup. Label 1 is the source aperture, label 2 is the sample material at angle θ to the incident beam, label 3 is the detector. Source: [4]. **Right:** Diffraction results for LiF. On the x-axis, we have the angle of diffraction θ . On the y-axis, we have logarithm of the detected rate of X-rays.

The interplanar spacing d is determined by the type of crystal we observe and the direction we take as normal. Since the crystal planes are physical planes that intersect atoms, we can determine the rules for the allowed sets of crystal planes and their respective values of d . These are given by the *Miller indices*; the rules for which Miller indices are allowed depending on the crystal can be found in [4]. This gives us the following relationship:

$$\frac{1}{d^2} = \frac{h^2}{a^2} + \frac{k^2}{b^2} + \frac{l^2}{c^2}, \quad \text{for cubic lattice: } \frac{1}{d^2} = \frac{h^2 + k^2 + l^2}{a^2}. \quad (11)$$

Here a , b , and c are lattice parameters and h , k , and l are integers.

First, we measure the values of a for two BCC crystals - LiF and NaCl. The crystals have been cut so that the flat exposed part is the $(h, k, l) = (1, 0, 0)$ family of planes, hence $d = a$, and are FCC (face-centred cubic) crystals. The lattice constants measured are:

$$\text{LiF: } a = 403.9(6) \text{ pm} \quad \text{NaCl: } a = 564.9(8) \text{ pm}. \quad (12)$$

Then, we measured the values of a for two semiconductor samples X2, Y2. We know that their crystal structure is zincblende, which has the same primitive FCC lattice. We also know they are cut so that the flat exposed part is the $(h, k, l) = (1, 1, 1)$ family of planes, hence $d = a/\sqrt{3}$. We measure the lattice constants as:

$$\text{X2: } a = 585.65(87) \text{ pm} \quad \text{Y2: } a = 648.57(94) \text{ pm}. \quad (13)$$

Comparing to a database of semiconductors, we find that the samples are as follows: X2 is InP with $a = 586.87$ pm and Y2 is InSb with $a = 647.9$ pm.

Appendix B Energy spectra plots

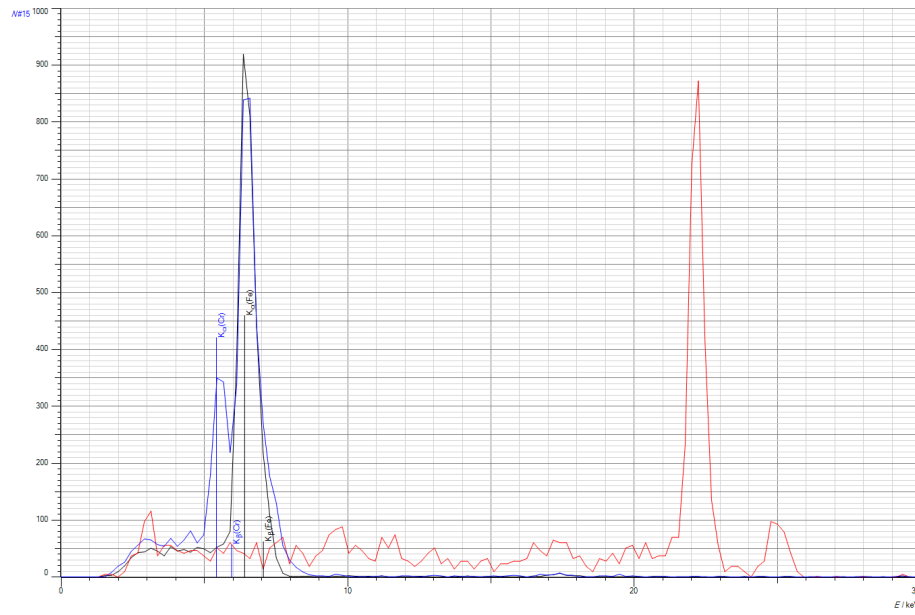


Figure B2: Spectrum of sample b1-1. Calibration spectra of Fe and Ag in black and red respectively. It can be seen that the sample consists of Fe and Cr, and their spectra overlap. This presents a difficulty in fitting emission lines.

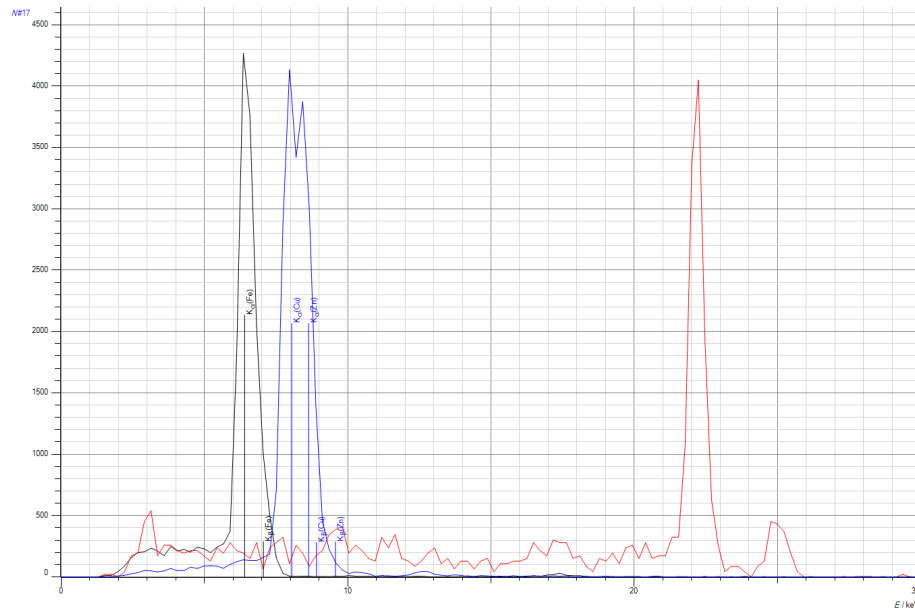


Figure B3: Spectrum of sample b1-3. Calibration spectra of Fe and Ag in black and red respectively. It can be seen that the sample consists of Cu and Zn, and their spectra overlap significantly. This presents a difficulty in fitting emission lines.

Appendix C Official Coin Data

We present the official data of the coin composition given by the coin issuing officials in Table C1. The sources for the coins per country of origin are: UK [12], Singapore [13, 14], EU [15], Norway [16], Switzerland [17], Sweden [18], Japan [7], Hong Kong [19], USA [20], Canada [8].

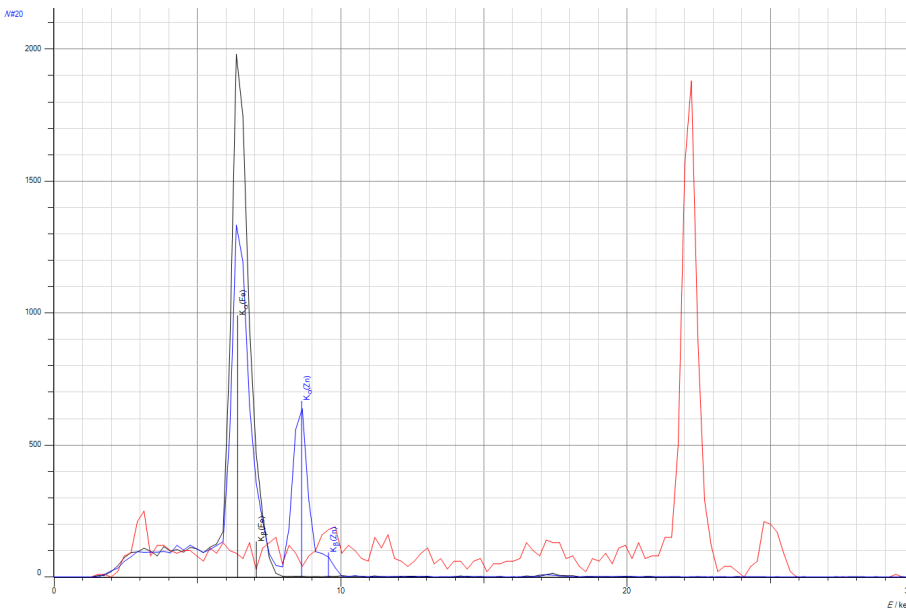


Figure B4: Spectrum of sample b2-c. Calibration spectra of Fe and Ag in black and red respectively. It can be seen that the sample consists of Fe and Zn, and their spectra do not overlap.

No	Country	Denomination	Ni, %	Cu, %	Zn, %	Other, %	Weight, g
3	United Kingdom	50p old	25	75	0	0	8
4	United Kingdom	50p new	25	75	0	0	8
5	United Kingdom	20p new	16	84	0	0	5
6	United Kingdom	10p old	25	75	0	0	6.5
7	United Kingdom	10p new	6	0	0	mild Steel - 94	6.5
8	United Kingdom	2p new	0	6	0	mild Steel - 94	7.12
9	Singapore	1 dollar old	2	92	0	Al - 6	8.05+-0.20
10	Singapore	50c old	25	75	0	0	8.56+-0.20
11	Singapore	20c new	?	0	0	steel - ?	6.56+-0.28
12	Bulgaria	50 stotinki	10			0	5
13	Bulgaria	5 stotinki				steel - ?	3.5
14	European Union	50c	0	89	5	Al - 5, Sn - 1	7.8
15	European Union	2c old	0	plating	0	steel core	3.06
16	European Union	2c new	0	plating	0	steel core	3.06
17	Romania	10 bani	?	0	0	steel - ?	4
18	Norway	1 krone	25	75	0	0	4.35
19	Switzerland	20 centim	25	75	0	0	4
20	Sweden	1 krona	25	75	0	0	7
21	Japan	1 yen	0	0	0	al-100	1
22	Hong Kong	10c				0	1.85
23	Uganda	200 schillings	~30	~70	0	0	8.5
24	USA	25c	8.33	91.66		0	5.670
25	USA	1c	0	2.5	97.5	0	2.5
26	Canada	25c	2.2	3.8	0	steel - 94	4.4
27	Brazil	5 centavos	0			0	

Table C1: Table of official info about the international coins. Notable are the coins with predominantly steel composition with a coating of one of the three main elements.